Journal of Physics B: Atomic, Molecular and Optical Physics

PAPER

Deep minima and vortices for positronium formation in low-energy positron-hydrogen collisions

IOP Publishing Journal of Physics B: Atomic, Molecular and Optical Physics
J. Phys. B: At. Mol. Opt. Phys. **52** (2019) 205201 (11pp) https://doi.org/10.1088/1361-6455/ab31f6

Deep minima and vortices for positronium formation in low-energy positron-hydrogen collisions

Albandari W Alrowaily[1,3], S J Ward[1] and P Van Reeth[2]

[1] Department of Physics, University of North Texas, Denton, TX 76203, United States of America
[2] Department of Physics and Astronomy, University College London, Gower Street, London WC1E 6BT, United Kingdom

E-mail: Sandra.Quintanilla@unt.edu

Received 23 April 2019, revised 13 June 2019
Accepted for publication 12 July 2019
Published 30 September 2019

Abstract

Using the two-channel Kohn and inverse Kohn variational methods, we investigate ground-state positronium (Ps) formation in positron-hydrogen collisions in the Ore gap. We find two zeros in the Ps-formation scattering amplitude f_{Ps} and corresponding deep minima in the Ps-formation differential cross section (DCS), and we determine their positions accurately. Due to azimuthal symmetry, each zero in f_{Ps} is part of separate circular rings of zeros for an azimuthal angle range of zero to 2π. We study the velocity field associated with f_{Ps} in which we treat the magnitude of the momentum of the incident positron and the angle of the outgoing positronium as variables, and we refer to this velocity field as the extended velocity field. We show that it has two vortices that are connected with the zeros in f_{Ps}, and that it rotates in opposite directions around the two zeros in f_{Ps}. Previously, vortices in the velocity field associated with the transition matrix element have provided an explanation for deep minima in DCSs for direct ionization. With the introduction of the extended velocity field, our work shows that vortices can occur also for charge exchange.

Keywords: positron collisions, vortices, positronium, charge exchange

(Some figures may appear in colour only in the online journal)

1. Introduction

In atomic physics one is interested in structures in differential cross sections (DCSs). Currently, there is an interest in deep minima in the triply differential cross section (TDCS) for ionization by electron or positron impact and in their interpretation in terms of vortices. Recently, Macek *et al* [1] provided an explanation for a deep minimum in the TDCS measurements of electron-helium ionization [2] in terms of a vortex. Their work led to interest in vortices for ionization by electron and positron impact. For instance, Ward and Macek [3] examined K-shell ionization of a model carbon atom by fast electron impact using the Coulomb–Born approximation and noted a vortex in the velocity field associated with the transition matrix element. Also, Navarrete *et al* [4] and Navarrete and Barrachina [5, 6] found deep minima in the fully DCS for positron-impact ionization of atomic hydrogen. They established that the deep minima are due to zeros in the transition matrix element and that the zeros are related to vortices in the generalized velocity field associated with this element [5–7]. Navarrete and Barrachina [5–7] found a pair of zeros, and they noticed that the velocity field rotates in opposite directions around the two zeros.

Vortices have also been discussed for ionization by other projectiles. Macek *et al* [8] performed a time-dependent calculation of proton-hydrogen collisions and addressed vortices associated with zeros in a single-particle wave function and with zeros in the momentum distribution of the ionized electron. They discussed the transfer of angular momentum for the collision. Macek *et al* [8] and Macek [9] discussed ring vortices [10] and Macek [9] noted that there

[3] Home Institution: Princess Nourah bint Abdulrahman University, PO Box 84428 Riyadh, Saudi Arabia.

may be ring vortices associated with the first-Born approximation (FBA) treatment of high-velocity collisions. Recently, Ovchinnikov *et al* [11] considered a time-dependent wave function that was a superposition of two states, 1s and $2p_+$, of atomic hydrogen, and showed rotation of the probability density distribution around a zero. Citations of papers on vortices for ionization by ions, antiprotons and photons are given in [3]. Very recently, Ngoko Djiokap *et al* [12, 13] have studied electron vortices in ionization by circularly polarized UV pulses and Larionov *et al* [14] have considered vortices for ionization of a hydrogen-like atom by an ultrashort electromagnetic pulse. We note that McCullough *et al* [15] found a vortex for the collinear $H + H_2$ chemical exchange reaction [16], and Kuppermann *et al* [17] discussed vortices in stream lines plots for this reaction.

Dirac [18] showed that quantized vortices can occur around nodes of wave functions where the associated field would be a quantum probability field. Hirschfelder *et al* [16, 19], using Madelung's [20] hydrodynamical interpretation of quantum mechanics, connected vortices associated with single-particle wave functions to those in fluid dynamics (see Ghosh and Deb [21]). The hydrodynamic formulation of wave mechanics considers the flow of a quantum mechanical probability, and the derivation depends on the wave function being single-valued and continuous [10, 16, 19, 20]. (Wallace [22] presented carefully the case that a quantization condition should be included with Madelung's hydrodynamic equation to obtain the Schrödinger equation. Navarrete and Barrachina [6] noted that there is a controversy regarding the equivalence of these equations [6, 22, 23].) The dynamics of vortices in velocity fields associated with wave functions have been studied in detail by Bialynicki-Birula *et al* [10], who used the quantum hydrodynamic approach of Madelung [20] and considered both unbound vortex lines and vortex rings. Importantly, they related the vortices present in the velocity field to zeros in a single-particle complex wave function that is a solution to the time-dependent Schrödinger equation. Since the scattering wave function in coordinate space at asymptotic times can be connected to the momentum-space wave function through the imaging theorem [4–7, 24–28], zeros in the coordinate-space wave function can be mapped as zeros in the momentum-space wave function. Therefore, vortices in the velocity field associated with zeros in the coordinate-space scattering wave function at asymptotic times are evidenced as zeros in the momentum distribution, which is a quantity that may be experimentally assessable.

In this paper, we present two isolated first-order zeros in Ps-formation scattering amplitude $f_{\rm Ps}$, and two corresponding deep minima in the Ps-formation DCS, for positron-hydrogen collisions in the Ore gap. We connect the zeros to vortices in an extended velocity field associated with $f_{\rm Ps}$ when both k and θ in $f_{\rm Ps}$ are allowed to vary, where k is the magnitude of the momentum of the incident positron and θ is the angle of the outgoing Ps. We determine $f_{\rm Ps}$ using the two-channel K-matrices that we calculate using the Kohn and inverse Kohn variational methods, which are nonperturbative methods and are known to be capable of providing very accurate results if flexible trial functions are used [29, 30]. The Ore gap for positron-atom collisions is the energy region between the threshold for ground-state Ps formation and the first excitation threshold of the target atom, where the only channels open are elastic scattering and Ps(1s) formation (ignoring annihilation) [29, 31]. For positron-hydrogen collisions, the energy range of the incident positron for the Ore gap is 6.8–10.2 eV ($k = 0.7071$ to 0.8660 a.u.). While no experimental measurements have been made of the absolute Ps-formation DCS for positron collisions with atomic hydrogen, they have recently been obtained for He, Ar, H_2 and CO_2 near the forward direction [32]. The work that we present in this paper may be of interest to the atomic physics community due to the studies of structures in DCSs, the new experimental measurements of the Ps-formation DCS [32] and the recent literature on vortices for atomic ionization [1, 3–9, 11–14].

The advantage of obtaining zeros in the scattering amplitude for charge exchange rather than for atomic ionization is that there are fewer degrees of freedom. Ground-state Ps formation in positron collisions from ground-state atomic hydrogen is an example of charge exchange. For this process, when one takes the z-axis to be parallel to the direction of the incident positron, the scattering amplitude for this process, $f_{\rm Ps}$, depends only on the physical quantities k and θ.

The theoretical existence of narrow minima in the DCS for Ps formation in positron-hydrogen collisions has been presented by Drachman *et al* [33]. They calculated the Ps-formation DCS using the two-state coupled static approximation with correlation [34, 35] for the first two partial waves and the Born approximation for the higher partial waves. Mandal *et al* [36] applied the distorted-wave approximation (DWA), the distorted-wave polarization approximation (DWPA), and the FBA to Ps formation in positron-hydrogen collisions. They obtained a minimum in the DCS that corresponds in energy, 10.2 eV, to the second minimum that Drachman *et al* [33] obtained, but the angles determined with the various approximations are different. The DWA and FBA are not expected to be reliable at such a low energy, and one should not expect the DWPA to provide accurate results at low energies. Using the inverse Kohn and Kohn variational methods, we provide an accurate determination of the positions of deep minima in the Ps-formation DCS.

The outline of our paper is as follows. In section 2, we present the theory of the scattering calculations for Ps formation in positron-hydrogen collisions in the Ore gap, where we give an outline of the Kohn variational method and the s-wave trial function. In section 3, we discuss the numerical investigation of the K-matrices and we present our results in section 4. Specifically, in section 4.1 we give our results of the deep minima in the Ps-formation DCS and the positions of the zeros in $f_{\rm Ps}$, whereas in section 4.2 we define the velocity field associated with $f_{\rm Ps}$ and discuss the extended velocity field $\boldsymbol{v}_{\rm ext}$, including vortices associated with this field. We summarize our findings in section 5. In appendix A, we review the velocity field $\boldsymbol{v}$ associated with the transition amplitude for ionization and we give a similar expression for the velocity field $\boldsymbol{v}$ that is associated with the Ps-formation

scattering amplitude $f_{\rm Ps}$. Finally, in appendix B, we relate first-order zeros in $f_{\rm Ps}$ to vortices in $\boldsymbol{v}_{\rm ext}$.

We use atomic units throughout unless explicitly stated otherwise, and we quote the angle θ of the outgoing Ps in degrees.

2. Theory of the scattering calculations

We use the Kohn and inverse Kohn variational methods to evaluate K-matrices for ground-state Ps formation in positron-hydrogen collisions in the Ore gap. The Kohn variational method is described in detail in the papers [29, 30, 37, 38]. Here, we present an outline of the Kohn variational method and the form of the wave function specifically for s-wave scattering. The two-channel stationary Kohn functional from which the variational values of the K-matrix elements, K^v_{ij}, can be determined using the trial values of the K-matrix elements, K^t_{ij}, and the two components of the trial function (Ψ^t_1 and Ψ^t_2) has the form

$$\begin{bmatrix} K^v_{11} & K^v_{12} \\ K^v_{21} & K^v_{22} \end{bmatrix} = \begin{bmatrix} K^t_{11} & K^t_{12} \\ K^t_{21} & K^t_{22} \end{bmatrix} - \begin{bmatrix} (\Psi^t_1, L\Psi^t_1) & (\Psi^t_1, L\Psi^t_2) \\ (\Psi^t_2, L\Psi^t_1) & (\Psi^t_2, L\Psi^t_2) \end{bmatrix}, \quad (1)$$

where $L = 2(H - E)$ in which H is the total Hamiltonian of the positron-hydrogen system and E is the corresponding total energy. The functional is for all partial waves but, for simplicity of notation, we omit the partial wave ℓ on the K-matrix elements and on the components of the trial wave function. For s-wave scattering, following [29, 30], we choose for the two components of the trial product-form wave function to have the form:

$$\begin{aligned} \Psi^t_1 &= Y_{0,0}(\hat{\boldsymbol{r}}_1)\phi_{\rm H}(r_2)\sqrt{k}\,\{j_0(kr_1) - K^t_{11}n_0(kr_1)f_{sh}(r_1)\} \\ &\quad - Y_{0,0}(\hat{\boldsymbol{\rho}})\phi_{\rm Ps}(r_{12})\sqrt{2\kappa}\,K^t_{21}n_0(\kappa\rho)f_{sh}(\rho) \\ &\quad + \phi_{\rm H}(r_2)\sum_{i=1}^{N} c_i\phi_i \\ \Psi^t_2 &= Y_{0,0}(\hat{\boldsymbol{\rho}})\phi_{\rm Ps}(r_{12})\sqrt{2\kappa}\,\{j_0(\kappa\rho) - K^t_{22}n_0(\kappa\rho)f_{sh}(\rho)\} \\ &\quad - Y_{0,0}(\hat{\boldsymbol{r}}_1)\phi_{\rm H}(r_2)\sqrt{k}\,K^t_{12}n_0(kr_1)f_{sh}(r_1) \\ &\quad + \phi_{\rm H}(r_2)\sum_{j=1}^{N} c_j\phi_j, \end{aligned} \quad (2)$$

where $\phi_{\rm H}(r_2) = \pi^{-1/2}e^{-r_2}$ and $\phi_{\rm Ps}(r_{12}) = (8\pi)^{-1/2}e^{-r_{12}/2}$ are the ground-state wave functions of hydrogen and positronium, respectively. The position vectors of the positron and the electron with respect to the proton (which is treated as infinitely massive) are $\boldsymbol{r}_1$ and $\boldsymbol{r}_2$, respectively, and $r_{12} = |\boldsymbol{r}_1 - \boldsymbol{r}_2|$. In equation (2), $\boldsymbol{\rho} = (\boldsymbol{r}_1 + \boldsymbol{r}_2)/2$ is the center of mass position vector for the positronium with respect to the proton. The momenta of the incident positron and the outgoing Ps are given by $\boldsymbol{k}$ and $\boldsymbol{\kappa}$, respectively. The magnitude of these momenta are related through energy conservation according to

$$E = \frac{k^2}{2} - \frac{1}{2} = \frac{\kappa^2}{2M_{\rm Ps}} - \frac{1}{4}, \quad (3)$$

where $M_{\rm Ps} = 2$ a.u., the mass of the outgoing Ps atom. The Hylleraas-type short-range terms ϕ_j in equation (2) are given by

$$\phi_i = e^{-(\alpha r_1 + \beta r_2 + \gamma r_{12})} r_1^{k_i} r_2^{l_i} r_{12}^{m_i}, \quad (4)$$

where α, β and γ are nonlinear parameters, and k_i, l_i and m_i are nonnegative integer powers. (We choose $\alpha > 0$, $\gamma > 0$, and $\beta > -1$.) The coefficients c_i ($i = 1 \rightarrow N$) in equation (2) are linear variational parameters. We obtain the number of terms N in each sum in equation (2) by selecting the value of ω, where ω is a nonnegative integer given by $k_i + l_i + m_i \leqslant \omega$ [29, 30]. For $\omega = 6, 7, 8, 9$ and 10, $N = 84$, 120, 165, 220, and 286, respectively. The shielding functions $f_{sh}(\rho)$ and $f_{sh}(r_1)$ ensure that the singularities at the origin in the spherical Neumann functions $n_0(\kappa\rho)$ and $n_0(kr_1)$, respectively, are removed. A functional similar to equation (1) gives rise to the inverse Kohn variational method [29, 38], which we primarily use as we find empirically that it is less affected by the Schwartz singularities [39, 40]. We do compare the K-matrices and the positions of the zeros in $f_{\rm Ps}$ that we obtain using both variational methods to gauge the accuracy of these results.

If one takes the z-axis to be parallel to the momentum of the incident positron, then, due to azimuthal symmetry about the z-axis, the scattering amplitude for Ps(1s) formation $f_{\rm Ps}$ can be expanded in terms of Legendre polynomials according to [41]

$$f_{\rm Ps}(k, \theta) = \sqrt{\frac{M_{\rm Ps}}{k\kappa}} \sum_{\ell} (2\ell + 1) T^{\ell}_{12} P_{\ell}(\cos\theta), \quad (5)$$

where θ is the angle of the outgoing Ps. T^{ℓ}_{12} is the ℓth partial-wave T-matrix element for Ps formation which can be determined from the ℓth partial-wave K-matrix $\boldsymbol{K}^{\ell}$ according to [41]

$$T^{\ell}_{12} = \left[\frac{\boldsymbol{K}^{\ell}}{1 - i\boldsymbol{K}^{\ell}}\right]_{12}. \quad (6)$$

The azimuthal symmetry of the scattering means that $f_{\rm Ps}$ depends only on two physical quantities, which may be chosen to be (k, θ), or (κ_z, κ_x), where κ_z and κ_x are the z- and x-components of $\boldsymbol{\kappa}$, respectively, and the x-axis is in the scattering plane of $\boldsymbol{k}$ and $\boldsymbol{\kappa}$ and to the left of the z-axis. The Ps-formation DCS is related to $f_{\rm Ps}$ by

$$\frac{d\sigma_{\rm Ps}}{d\Omega} = \frac{\kappa}{M_{\rm Ps}k}|f_{\rm Ps}(k, \theta)|^2 \quad (7)$$

with the ratio of ortho-Ps to para-Ps being 3:1 [37].

3. Numerical investigation of the variational *K*-matrices

The present calculations for the K-matrices extend the variational calculations of Humberston *et al* [30] for the s-, p- and d-waves to higher partial waves. An error in the d-wave calculation of [30] had recently been corrected as reported in Woods *et al* [38] and Van Reeth *et al* [42]. We calculate the f-wave K-matrix elements using sets of short-range terms in

the trial wave function with the three units of angular momentum on either the positron or the electron and a set in which one unit is associated with the electron and two with the positron [29, 30, 37, 43]. Using only short-range terms with all angular momentum on either the positron or the electron we also calculate three higher partial waves (the g-, h- and i-waves). We restrict the flexibility of the wave function for these partial waves since their contributions to $f_{\rm Ps}$ and to the corresponding DCS are not expected to be very large in the energy range of the Ore gap. We think that the inclusion of all possible sets of short-range terms in which the angular momentum is shared between the positron and the electron, following the procedure of Schwartz [43], is not warranted given the significant amount of extra work it would involve. For each symmetry that we consider in the trial function for a particular partial wave, we use the same number of short-range terms.

Due to near-linear dependence between terms in the wave function we encounter numerical issues with the evaluation of the higher partial-waves contributions which restrict the number of short-range terms we can include [39, 40]. With our selection of the ω values for the different partial waves, we obtain in the vicinity of the zeros in $f_{\rm Ps}$ inverse Kohn matrix elements that are smooth functions of k. We compute the K-matrices on a very fine grid in k in the vicinity of each of the two zeros in $f_{\rm Ps}$. In the vicinity of the first zero, we include the first four partial waves and consider the ω values 10, 9, 8, and 8 for $\ell = 0$, 1, 2 and 3, respectively. However, in the vicinity of the second zero, and for calculations over a wider range of k in the Ore gap, we include the first seven partial waves and consider the ω values of 9, 9, 8, 8, 7, 7, and 7 for $\ell = 0$, 1, 2, 3, 4, 5 and 6, respectively.

Since the K-matrices from the inverse Kohn method are generally more stable than those from the Kohn method, we use the inverse Kohn K-matrices for the results that we give in section 4, except for the comparison of the positions of the zeros that we obtain using the two methods. We find that at the positions of the two zeros in $f_{\rm Ps}$, for the first four partial waves the Kohn and inverse Kohn K-matrices agree very well; their difference is less than 0.63%. At the position of the second zero, the agreement between the K-matrices from the two methods is not as good for the higher partial waves as for the lower partial waves. For the g- and h-waves, we find that the difference is about 6% or less, and for the i-wave that the difference is within 14%. However, these higher partial waves contribute less significantly to the values of the positions of the zeros in $f_{\rm Ps}$ than do the lower partial waves together.

We estimate uncertainties in the inverse Kohn K-matrix elements by computing the percentage ratio $R_{ij} = (K_{ij}(\omega) - K_{ij}(\omega - 1))/K_{ij}(\omega - 1) \times 100\%$, where $K_{ij}(\omega)$ are the K-matrix elements at a particular ω value that we use in the calculation. We compute this percentage ratio at the positions of the two zeros. For the $\ell = 0$, 1 and 2 partial waves, this ratio is within 2% except at the position of the first zero where for the d-wave the ratio for K_{12} is within 3% and for K_{22} is within 18%. For the $\ell = 3$ partial wave, we find that for all matrix elements the ratio is within 2% except at the position of the second zero where the ratio for K_{22} is about 50%. In general, we do not achieve the same accuracy and confidence in the K-matrices for the $\ell > 3$ partial wave as for the lower partial waves.

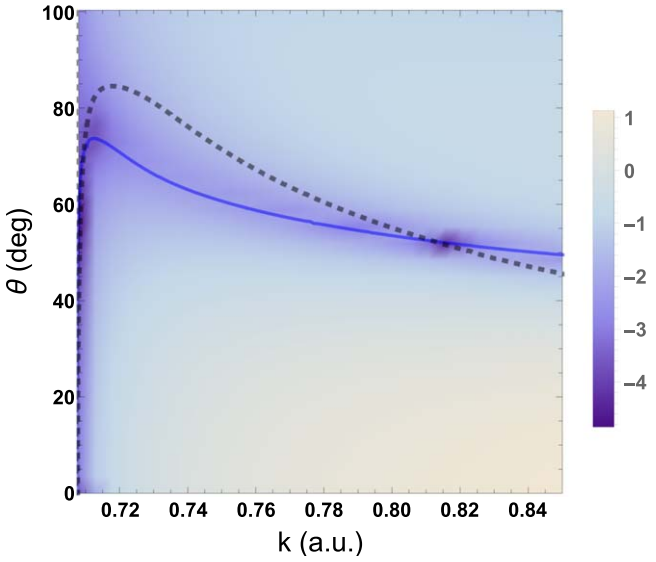

Figure 1. The common logarithm of the Ps-formation differential cross section, $\log_{10}$[DCS], as a function of k and θ, for positron-hydrogen collisions over the most of the Ore gap. The nodal lines of Re[$f_{\rm Ps}$] = 0 and Im[$f_{\rm Ps}$] = 0 are shown by the solid blue line and the dashed black line, respectively.

4. Results

4.1. Deep minima in the Ps-formation DCS and positions of the zeros in the Ps-formation scattering amplitude f_{Ps}

In figure 1, we show the Ps-formation DCS and the nodal lines of Re[$f_{\rm Ps}$] = 0 and Im[$f_{\rm Ps}$] = 0 as functions of k and θ. The nodal line of Re[$f_{\rm Ps}$] follows a region where the Ps-formation DCS is very small, starting rapidly from threshold up to a maximum and then decreasing slowly with increasing k. The nodal line of Im[$f_{\rm Ps}$] intercepts the nodal line of Re[$f_{\rm Ps}$] at two points at which $f_{\rm Ps}$ is zero. The first zero of $f_{\rm Ps}$ lies very close to threshold, and the second one lies in the region where the nodal line of Re[$f_{\rm Ps}$] does not vary much with θ. A three-dimensional plot of the common logarithm of the Ps-formation DCS, figure 2(a), reveals two deep and narrow minima, one near threshold at $k = 0.7095$ and the other at $k = 0.8124$. These minima can be seen more closely in the three-dimensional plots of figures 2(b) and (c), respectively. We show a two-dimensional plot of the logarithm of the Ps-formation DCS as a function of θ for $k = 0.7095$ and 0.8124 in figures 3(a) and (b), respectively. In figure 3(a) the deep minimum occurs at 70.8°, while in figure 3(b) it occurs at a smaller angle of 52.3°.

Drachman *et al* [33] performed a pioneering calculation of the Ps-formation DCS for positron-hydrogen collisions. For the first two partial waves they used the K-matrices from the coupled static approximation with correlation [34, 35], and for the higher partial waves they used the Born

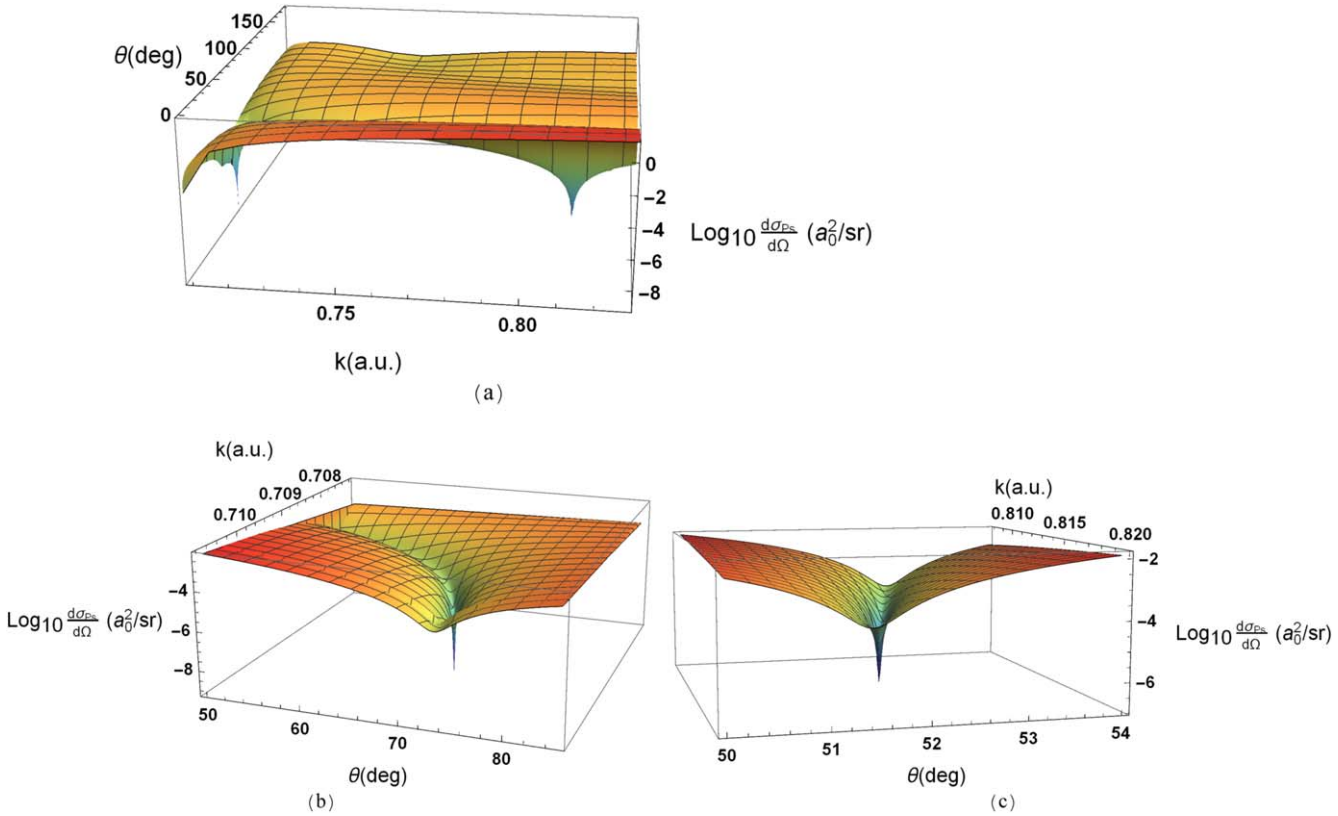

Figure 2. The common logarithm of the Ps-formation differential cross section for positron-hydrogen collisions as a function of k and θ. (a) shows two deep minima in the k range of 0.708–0.83, (b) shows the first deep minimum and (c) shows the second deep minimum.

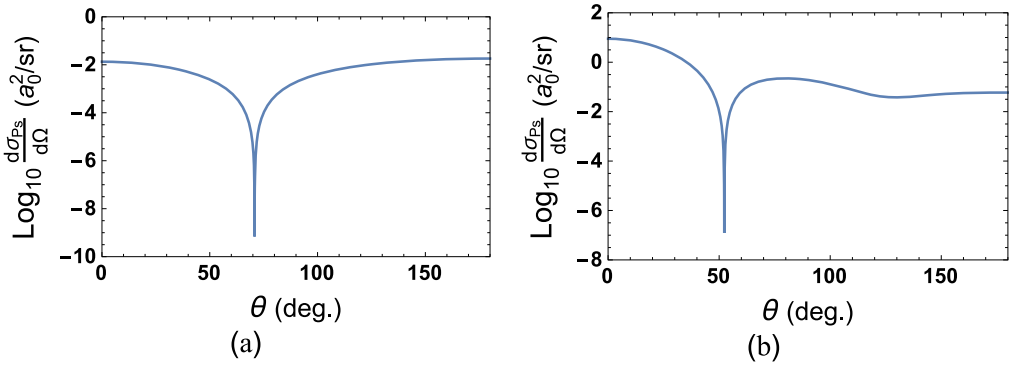

Figure 3. The common logarithm of the Ps-formation differential cross section, $\log_{10}$[DCS], as a function of θ for $k = 0.7095$ (a) and for $k = 0.8124$ (b).

Table 1. Comparison of the positions (k_0, θ_0) of the zeros in f_{Ps} from the inverse Kohn and Kohn K-matrices. (a) First zero, (b) Second zero.

Method	k_0	θ_0 (deg.)
(a)		
Inverse Kohn	0.7095	70.8
Kohn	0.7095	70.7
(b)		
Inverse Kohn	0.8124	52.3
Kohn	0.8110	52.6

approximation. They obtained narrow minima in the Ps-formation DCS, one at ($k_0 = 0.80$, $\theta_0 = 57°$) and another at ($k_0 = 0.866$, $\theta_0 = 51°$), where $k = 0.866$ is the first excitation threshold of $H(n = 2)$. The position of the second deep minimum that we obtain using the inverse Kohn variational method is comparable to the position of the first minimum that Drachman *et al* [33] obtained using a simpler approximation, although the minimum we obtain is orders of magnitude deeper. Drachman *et al* [33] did not report the first deep minimum that we obtain using a fine mesh in k.

In table 1, we compare the positions (k_0, θ_0) of the two zeros in f_{Ps} that we obtain using the inverse Kohn and Kohn variational methods. For the position of the first zero, the k_0

Table 2. Convergence of the k_0 and θ_0 positions of the first and second zeros in f_{Ps} with respect to the maximum partial wave, ℓ_{max} in f_{Ps}. (a) First zero, (b) Second zero.

ℓ_{max}	k_0	θ_0 (deg.)
(a)		
1	0.7102	77.5
2	0.7096	71.2
3	0.7095	70.8
(b)		
2	0.779	65.7
3	0.797	56.6
4	0.8102	52.9
5	0.8138	52.0
6	0.8124	52.3

Table 3. Convergence of the (k_0, θ_0) positions of the first and second zeros in f_{Ps} with respect to $\omega' = \omega - i$, where $i = 0$, 1 and 2, and ω is related to the number of terms in each sum in the components of a trial partial-wave scattering wave function in the full calculation (see section 3 and the last paragraph of section 4.1). (a) First zero, (b) Second zero.

ω'	k_0	θ_0 (deg.)
(a)		
ω	0.7095	70.8
$\omega - 1$	0.7095	70.6
$\omega - 2$	0.7095	71.1
(b)		
ω	0.8124	52.3
$\omega - 1$	0.8112	52.2
$\omega - 2$	0.8144	51.9

values agree to four significant figures between the two methods and the θ_0 values differ by less than 0.15%. The difference between the two methods is slightly more for the second zero: the k_0 values differ by less than 0.2% and the θ_0 values by less than 0.6%. Thus, we conclude that the values of the positions of the zeros determined by the inverse Kohn and Kohn variational methods are close. In tables 2 and 3, and in the figures, we use the inverse Kohn results.

Each zero in f_{Ps} given in table 1 is one of a pair of zeros that intersects the $\kappa_y = 0$ plane. One zero of the pair occurs at the azimuthal angle of $\varphi = 0$, or at $\kappa_z = \kappa_{z0}$, $\kappa_x = \kappa_{x0}$ (which is the zero given in the tables), while the other due to azimuthal symmetry occurs at $\varphi = \pi$, or at $\kappa_z = \kappa_{z0}$, $\kappa_x = -\kappa_{x0}$. Due to azimuthal symmetry each pair of zeros is associated with a circular ring of zeros in f_{Ps}, and in the Ps-formation DCS, about the z-axis. Since we find two zeros in f_{Ps}, we conclude that there are two distinct circular rings of zeros in the Ore gap.

Table 2 shows the convergence of the positions of the zeros in f_{Ps} with respect to the maximum partial wave, ℓ_{max}, that we include in the truncated sum of f_{Ps}, equation (5).

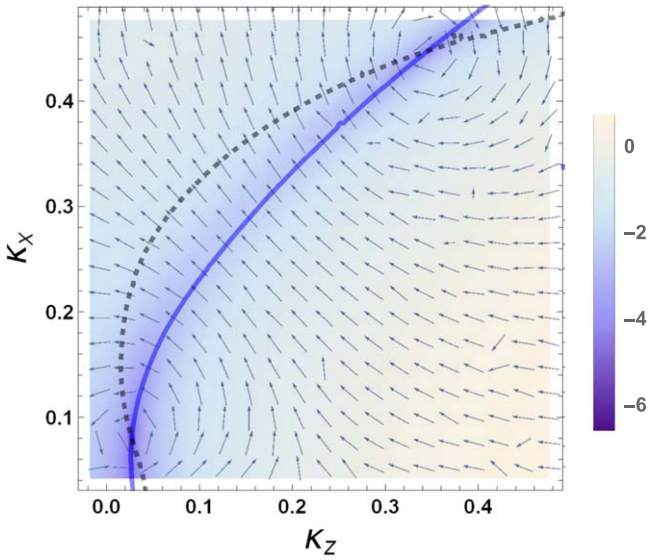

Figure 4. Unit vector of the extended velocity field $\hat{\boldsymbol{v}}_{ext}$ (solid blue arrows) associated with f_{Ps}, nodal lines of Re[f_{Ps}] (solid blue line) and Im[f_{Ps}] (dashed black line) and a density plot of $\log_{10}$[DCS] for Ps formation in positron-hydrogen collisions for a (κ_z, κ_x) grid that encloses both zeros in f_{Ps}. (There are some irregularities in the nodal lines and some anomalies in $\hat{\boldsymbol{v}}_{ext}$ that may be due to singularities in the K-matrices in this (κ_z, κ_x) grid.)

Interestingly, we obtain the first zero with only the first two partial waves while the first three partial waves are needed to obtain the second zero. For the first zero, the position of the first zero stays stable to three significant figures in k_0 and to two significant figures in θ_0 in increasing the number of partial waves from three to four. For the second zero, we find that the k_0 and θ_0 values of the position of the second zero are stable to two significant figures between including the first six partial waves and including the first seven.

Ps(1s)-formation in positron-hydrogen collisions is a particularly simple process for studying a zero in the scattering amplitude and corresponding DCS since only two partial waves are necessary to obtain the first zero. In contrast, for fast electron-impact ionization of inner-shell carbon, Ward and Macek [3] found that $\ell = 0$, 1 and 2, $m = 0$ and $\ell = 0$, $m \pm 1$ components of a multipole expansion of the transition matrix element (about the momentum transfer axis) are all necessary to obtain a deep minimum in the TDCS. Colgan *et al* [44] found that in a time-dependent close-coupling calculation of electron-impact ionization of helium for an incident electron energy of 64.6 eV at least the first three partial waves are needed to obtain a minimum in the TDCS. For this process, Feagin [45] expanded the scattering amplitude in cylindrical partial waves of the electron pair about the vortex singularity. His findings are similar to ours for the first zero in that, although the deep minimum in the cross section is obtained only with the first two terms in an expansion of the scattering amplitude, the inclusion of the next term significantly improves the results.

In table 3, we show the variation of the position (k_0, θ_0) of each zero in f_{Ps} with respect to $\omega' = \omega - i$, where $i = 0$, 1 and 2, and ω is related to the number of short-range terms N in each sum in the components of a trial partial-wave scattering

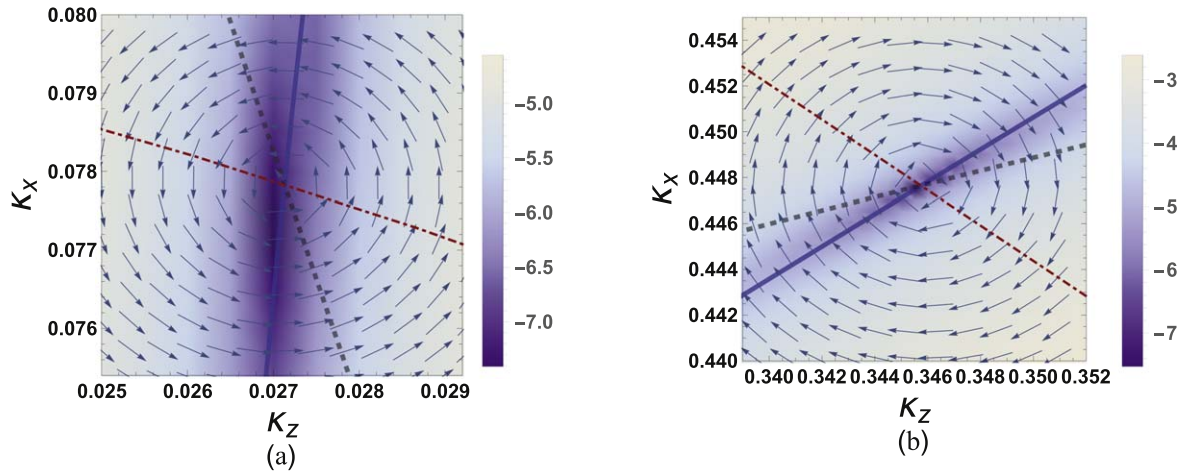

Figure 5. The common logarithm of the Ps-formation differential cross section $\log_{10}$[DCS], as a function of (κ_z, κ_x) for the region about a zero. The intersection of the nodal lines of Re$[f_{\rm Ps}] = 0$ (solid blue line) and Im$[f_{\rm Ps}] = 0$ (dashed black line) is at the zero in $f_{\rm Ps}$, $(\kappa_{z0}, \kappa_{x0})$. The solid blue arrows denote the unit vector of the extended velocity field $\hat{\boldsymbol{v}}_{\rm ext}$, for the grid (κ_z, κ_x). The arc of constant $\kappa_0 = \sqrt{\kappa_{z0}^2 + \kappa_{x0}^2}$ is shown by the red dotted–dashed line. (a): shows the region enclosing the first zero and (b): shows the region enclosing the second zero.

wave function that we use in the full calculation (see section 3 and equation (2) for the *s*-wave). The value of ω that we use for each partial wave in the full calculation is given in section 3. Although the convergence of the position of the zeros with respect to ω' is not monotonically convergent, these results indicate that the positions we obtain will not change significantly if even a larger calculation is undertaken. In comparison with the first zero, the second zero, for which we also include the *g*-, *h*- and *i*-waves, the differences that we obtain by reducing the ω' value by two are more significant.

4.2. Extended velocity field $\boldsymbol{v}_{\rm ext}(\kappa, \theta)$ associated with the Ps-formation scattering amplitude $f_{\rm Ps}$

In appendix A we give the equation, equation (A.3), for the velocity field associated with the transition amplitude for ionization that is from paper [26]. Using the terminology of this equation we write the velocity field $\boldsymbol{v}$ associated with the Ps-formation scattering amplitude $f_{\rm Ps}$ as

$$\boldsymbol{v} = \frac{1}{M_{\rm Ps}} \mathrm{Im}\, \nabla_{\boldsymbol{\kappa}} [\ln f_{\rm Ps}] = -\frac{i}{2M_{\rm Ps}} \left(\frac{f_{\rm Ps}^* \nabla_{\boldsymbol{\kappa}} f_{\rm Ps} - (\nabla_{\boldsymbol{\kappa}} f_{\rm Ps}^*) f_{\rm Ps}}{|f_{\rm Ps}|^2} \right). \tag{8}$$

In the vicinity of each zero, we determine the velocity field $\boldsymbol{v}$ that is associated with $f_{\rm Ps}$ for a fixed value of k, so that $\boldsymbol{v}(\kappa, \theta) = v_\theta(\kappa, \theta)\hat{\boldsymbol{\theta}}$, where $v_\theta(\kappa, \theta)$ is obtained from the $\hat{\boldsymbol{\theta}}$ component of $\nabla_{\boldsymbol{\kappa}}$. For the first zero, we find that for k slightly less than k_0, $v_\theta(\kappa, \theta_0)$ is negative, while for k slightly greater than k_0, it is positive. The opposite is the case for the second zero.

We extend the velocity field by treating both κ and θ as variables in $f_{\rm Ps}$ (see appendix B), and we refer to this quantity as the extended velocity field $\boldsymbol{v}_{\rm ext}$, where $\boldsymbol{v}_{\rm ext}(\kappa, \theta) = v_\theta(\kappa, \theta)\hat{\boldsymbol{\theta}} + v_\kappa(\kappa, \theta)\hat{\boldsymbol{\kappa}}$, and $v_\kappa(\kappa, \theta)$ is obtained from the $\hat{\boldsymbol{\kappa}}$ component of $\nabla_{\boldsymbol{\kappa}}$, respectively. In figure 4, we show a density plot of the common logarithm of the Ps-formation DCS, the nodal lines of Re$[f_{\rm Ps}]$ and Im$[f_{\rm Ps}]$ and the unit vector $\hat{\boldsymbol{v}}_{\rm ext} = \boldsymbol{v}_{\rm ext}/|\boldsymbol{v}_{\rm ext}|$ for a (κ_z, κ_x) grid that includes both zeros in $f_{\rm Ps}$, where we treat κ_z and κ_x as independent variables. The two zeros in $f_{\rm Ps}$ and in the Ps-formation DCS occur at the two intersections of the nodal lines of Re$[f_{\rm Ps}] = 0$ and Im$[f_{\rm Ps}] = 0$. Vortices occur in $\boldsymbol{v}_{\rm ext}$, as can be seen from the rotation of this quantity around the two isolated zeros.

For each zero in $f_{\rm Ps}$, we compute $f_{\rm Ps}$ and the Ps-formation DCS for a small grid in (κ_z, κ_x) that encloses the zero. In figures 5(a) and (b), we show for the first and second zeros, respectively, the nodal lines of $f_{\rm Ps}$ and the Ps-formation DCS. We obtain the position of a zero, $(\kappa_{z0}, \kappa_{x0})$, in $f_{\rm Ps}(\kappa_z, \kappa_x)$ from an intersection of the nodal lines.

In the vicinity of a zero we can expand $f_{\rm Ps}$ about each zero according to

$$f_{{\rm Ps},j}(\kappa_z, \kappa_x) = \sum_{i=1}^{j} a_{ij}(\kappa_z - \kappa_{z_0})^i + b_{ij}(\kappa_x - \kappa_{x_0})^i. \tag{9}$$

We substitute equation (9) into equation (8) to determine $\boldsymbol{v}_{\rm ext}$ in the vicinity of a zero. The term, $i = j = 1$ in equation (9), corresponds to the linear form equation (B.1) with $a_{11} = a$, $b_{11} = ab$. We find that, for the linear fit, Im$[b]$ = Im$[b_{11}/a_{11}]$ is positive for the first zero in $f_{\rm Ps}$ and negative for the second zero. We determine $f_{\rm Ps}$, $\boldsymbol{v}_{\rm ext}$, $\hat{\boldsymbol{v}}_{\rm ext} = \boldsymbol{v}_{\rm ext}/|\boldsymbol{v}_{\rm ext}|$, and the circulation Γ (see appendix B), by taking $j = \ell_{\rm max}$ in equation (9), where $\ell_{\rm max}$ is the maximum ℓ value that we use in the Legendre series of $f_{\rm Ps}$ in the vicinity of a zero (see section 3). In figures 5(a) and (b) we also show $\hat{\boldsymbol{v}}_{\rm ext}$ for the first and second zeros, respectively. The extended velocity field rotates about each zero in $f_{\rm Ps}$ and the rotation is in opposite directions for the two zeros. Thus, vortices are present in $\boldsymbol{v}_{\rm ext}$ that are associated with zeros in $f_{\rm Ps}$.

To evaluate the circulation Γ about each zero, we use equations (8), (9) and (B.3). We find that, as expected from appendix B, $\Gamma = 2\pi/M_{\rm Ps}$ for the first zero, indicating counterclockwise rotation, while $\Gamma = -2\pi/M_{\rm Ps}$ for the second zero, indicating clockwise rotation. Thus, the sum of the two circulations is zero for the two zeros in $f_{\rm Ps}$ that lie in the upper-half $\kappa_z - \kappa_x$ ($\kappa_x > 0$) plane. The sum of $\langle L_y \rangle_A$ for a

pair of zeros in $f_{\rm Ps}$ in the same circular ring of zeros in $f_{\rm Ps}$ in the $\kappa_z - \kappa_x$ plane is zero, where L_y is the y-component of the angular momentum operator and A is a small area (circle or square) whose center is at the zero (see appendix B). Using the linear expansion of $f_{\rm Ps}$, equation (B.1), we find that $\langle L_y \rangle_A > 0$ for the first zero and $\langle L_y \rangle_A < 0$ for the second zero, and interestingly, their sum is close to zero, even though these zeros are part of two different circular rings of zeros.

5. Summary

Using inverse Kohn K-matrices, we have accurately evaluated the positions of two zeros in the Ps(1s)-formation scattering amplitude $f_{\rm Ps}$ for positron-hydrogen collisions in the Ore gap, and, thus, in the corresponding Ps-formation DCS [46]. We have found that the first zero is very close to the Ps(1s)-formation threshold while the second zero is at $k = 0.812\,4$ a.u., which corresponds to an energy 2.18 eV above the threshold. The two zeros in $f_{\rm Ps}$ are associated with two different circular rings of zeros in $f_{\rm Ps}$ and in the Ps-formation DCS.

We have shown that there are vortices in the extended velocity field $\boldsymbol{v}_{\rm ext}$ associated with $f_{\rm Ps}$, and that this velocity field rotates around the zeros in opposite directions for the two zeros [46]. Thus, for the same charge of the incident projectile and for the same atomic process, the extended velocity field can rotate in opposite directions around zeros that are part of different circular rings. Previously, for positron-impact ionization, the velocity field has been shown to rotate in opposite directions for a pair of zeros that are part of the same vortex ring [5–7]. Our work shows importantly that vortices occur for a charge-exchange atomic process, and are therefore not restricted in atomic collisions to direct ionization (see section 1).

Acknowledgments

We appreciate discussions with Drs John Humberston, Gaetana (Nella) Laricchia, Serge Ovchinnikov, and David Schultz, and we acknowledge Dr Gaetana Laricchia for having instigated the present investigation. AWA is a scholarship holder from Princess Nourah bint Abdulrahman University. SJW is thankful for support from the NSF under Grant No. PHYS-1707792 and an UNT Physics Department Seed Grant in 2017. Computational resources were provided by UNT's High Performance Computing Services. Mathematica [47] was used for the figures and for the fitting of the Ps-formation scattering amplitude.

Appendix A. Velocity field for the transition amplitude for ionization and the velocity field v associated with the Ps-formation scattering amplitude $f_{\rm Ps}$

Vortices have been studied in the standard velocity field $\boldsymbol{v}$ that is defined in terms of the coordinate-space wave function $\Psi(\boldsymbol{r}, t)$ according to [3, 10, 16, 19]

$$\boldsymbol{v}(\boldsymbol{r}, t) = \frac{i}{2m}\frac{[\Psi(\boldsymbol{r}, t)\nabla\Psi^*(\boldsymbol{r}, t) - \Psi^*(\boldsymbol{r}, t)\nabla\Psi(\boldsymbol{r}, t)]}{|\Psi(\boldsymbol{r}, t)|^2} = \frac{1}{m}\,\mathrm{Im}\,\nabla[\ln\Psi(\boldsymbol{r}, t)], \tag{A.1}$$

where m is the mass of the particle, $\boldsymbol{r}$ is the position vector, t is time, and ∇ is the gradient operator. The coordinate-space wave function at asymptotic times is related to the momentum-space wave function through the imaging theorem [6, 26–28]. This theorem equates, within a phase factor and a normalization factor, the coordinate-space wave function, with $\boldsymbol{r}$ set equal to the classical value $\mathbf{v}_{ej}t$ in the asymptotic limit $t \to \infty$, to the momentum-space wave function $\Phi(\boldsymbol{k}_{ej}, t)$, which is the Fourier transform of $\Psi(\boldsymbol{r}, t)$ [6, 26–28]. Here,$\mathbf{v}_{ej}$ and $\boldsymbol{k}_{ej}$ are the velocity and momentum of an ejected particle for an infinite massive target nucleus, respectively. For a single particle, the imaging theorem can be written as

$$\lim_{t\to\infty}[|\Psi(\boldsymbol{r}, t)|^2 d\boldsymbol{r}]|_{\boldsymbol{r}=\mathbf{v}_{ej}t} = |\Phi(\boldsymbol{k}_{ej}, t)|^2 d\boldsymbol{k}_{ej} = P(\boldsymbol{k}_{ej})d\boldsymbol{k}_{ej}, \tag{A.2}$$

where $P(\boldsymbol{k}_{ej})$ is the momentum distribution which is time independent [1, 6, 24–28]. The general derivation of the relationship between the coordinate-space and momentum-space wave functions, from which equation (A.2) can be obtained, was derived by Kemble [24]. Recent derivations of the imaging theorem have been given by Macek [26] and by Briggs and Feagin [27, 28]. The imaging theorem shows that vortices in the velocity field associated with zeros in the coordinate-space wave function at asymptotic times are also associated with zeros in the momentum-space wave function.

Macek [26] gave an expression for the velocity field $\boldsymbol{v}(\mathbf{k}_e)$ that is associated with the transition amplitude $a_{\mathbf{k}_e i}$, namely,

$$\boldsymbol{v}(\mathbf{k}_e) = \mathrm{Im}\,\nabla_{\mathbf{k}_e}[\ln a_{\mathbf{k}_e i}], \tag{A.3}$$

where i specifies is the initial state of the electron, $\mathbf{k}_e$ is the momentum of the ejected electron whose mass is 1 a. u. and $\nabla_{\mathbf{k}_e}$ is in the gradient operator in momentum space. If $a_{\mathbf{k}_e i}$ has isolated first-order zeros, then vortices are present in the velocity field associated with this amplitude.

Using the terminology of equation (A.3) and of papers [3–6, 10], we write the velocity field $\boldsymbol{v}$ associated with the Ps-formation amplitude $f_{\rm Ps}$ as

$$\boldsymbol{v} = \frac{1}{M_{\rm Ps}}\,\mathrm{Im}\,\nabla_{\boldsymbol{\kappa}}[\ln f_{\rm Ps}] = -\frac{i}{2M_{\rm Ps}}\left(\frac{f_{\rm Ps}^*\nabla_{\boldsymbol{\kappa}} f_{\rm Ps} - (\nabla_{\boldsymbol{\kappa}} f_{\rm Ps}^*) f_{\rm Ps}}{|f_{\rm Ps}|^2}\right). \tag{A.4}$$

We also give this equation in section 4.2 where it is labeled as equation (8).

Appendix B. The extended velocity field v_{ext}, the circulation Γ, and the expectation value of the *y*-component of angular momentum $\langle L_y\rangle_A$ associated with a linear expansion of f_{Ps} about a first-order zero

We evaluate a velocity field $\boldsymbol{v}(\kappa, \theta) = v_\theta(\kappa, \theta)\hat{\boldsymbol{\theta}}$ using equation (A.4) for fixed k (and thus fixed κ), where we take the derivative with respect to θ only, and we briefly describe this velocity field in the first paragraph of section 4.2.

Below, and in section 4.2 after the first paragraph, we consider for Ps formation an extended velocity field $\boldsymbol{v}_{ext}$ in which we allow both the energy of the incident positron beam and the angle of the outgoing Ps to vary in f_{Ps}, whose functional dependency on these two physical quantities is known. The extended velocity field can be expressed as $\boldsymbol{v}_{ext}(\kappa, \theta) = v_\theta(\kappa, \theta)\hat{\boldsymbol{\theta}} + v_\kappa(\kappa, \theta)\hat{\boldsymbol{\kappa}}$, where v_κ is from the κ derivative in $\nabla_{\boldsymbol{\kappa}}$ of equation (A.4). Considering f_{Ps} to depend on two independent variables, κ and θ, or alternatively κ_z and κ_x, allows for the corresponding velocity field $\boldsymbol{v}_{ext}$ to rotate around a zero similar to the velocity field associated with the transition matrix element for ionization by electron or positron impact for fixed incident momentum [1, 3–6, 26]. For both processes, however, it is the deep minima in the DCS for a particular incident energy that, in principle, is the quantity that is experimentally assessible.

One can expand f_{Ps} about an isolated first-order zero $(\kappa_{z0}, \kappa_{x0})$, and near the zero, it has the linear form

$$f_{Ps}(\kappa_z, \kappa_x) \approx a[(\kappa_z - \kappa_{z_0}) + b(\kappa_x - \kappa_{x_0})] = a[\kappa_z' + b\kappa_x'], \tag{B.1}$$

where b is a complex number in which $\mathrm{Im}[b] \neq 0$ [1, 3, 9, 10, 16, 48–50]. In equation (B.1) ($\kappa_z' = \kappa_z - \kappa_{z0} = \kappa' \cos\alpha$, $\kappa_x' = \kappa_x - \kappa_{x0} = \kappa' \sin\alpha$) are the z' and x' components of the momentum of the outgoing Ps, $\boldsymbol{\kappa}'$, with respect to a zero in f_{Ps}, so that $\boldsymbol{\kappa}' = \boldsymbol{\kappa} - \boldsymbol{\kappa}_0$, where $\boldsymbol{\kappa}_0$ is the momentum of Ps atom at the zero in f_{Ps}. The angle α is the angle between the vector $\boldsymbol{\kappa}'$ and the z'-axis.

We obtain equation (B.1) by using the multichannel effective range theory of Ross and Shaw [51] for T_{12}^{ℓ} and then shifting the origin from the Ps-formation threshold ($\kappa_z = 0$, $\kappa_x = 0$) to the position of an isolated first-order zero $(\kappa_{z0}, \kappa_{x0})$ in f_{Ps}. Feagin [45] performed a similar expansion for the scattering amplitude for e^--He ionization about the position of an isolated first-order zero in the scattering amplitude.

Substituting the linear expansion of f_{Ps} equation (B.1) into equation (A.4), one obtains the dominant term $\boldsymbol{v}_d$ of $\boldsymbol{v}_{ext}$ in the vicinity of the zero [50]:

$$\begin{aligned}\boldsymbol{v}_d &= \left(\frac{\mathrm{Im}[b]}{M_{Ps}}\right)\frac{(\hat{\boldsymbol{x}}\kappa_z' - \hat{\boldsymbol{z}}\kappa_x')}{\kappa_z'^2 + |b|^2\kappa_x'^2 + 2\,\mathrm{Re}[b]\kappa_z'\kappa_x'} \\ &= \left(\frac{\mathrm{Im}[b]}{M_{Ps}}\right)\frac{\hat{\boldsymbol{y}} \times \hat{\boldsymbol{\kappa}}'}{\kappa'}\frac{1}{\cos^2\alpha + |b|^2\sin^2\alpha + \mathrm{Re}[b]\sin 2\alpha},\end{aligned} \tag{B.2}$$

where $\kappa' = |\boldsymbol{\kappa}'|$, $\hat{\boldsymbol{\kappa}}' = \boldsymbol{\kappa}'/\kappa'$ and $\hat{\boldsymbol{y}} = \hat{\boldsymbol{z}} \times \hat{\boldsymbol{x}}$. The direction of $\boldsymbol{v}_d$ is orthogonal to $\hat{\boldsymbol{\kappa}}'$ and its magnitude has a $1/\kappa'$ singularity [50]. The extended velocity field in the vicinity of the zero in f_{Ps} circulates about the zero, with a counterclockwise rotation if $\mathrm{Im}[b] > 0$ and a clockwise rotation if $\mathrm{Im}[b] < 0$. It is irrotational except at a zero in f_{Ps}, i.e. at $\kappa' = 0$ [10, 50].

Using $\boldsymbol{v}_d$ given in equation (B.2) and taking a circular contour c of small radius and counterclockwise orientation, enclosing the isolated first-order zero in f_{Ps}, one can show that the circulation Γ is given by [3, 6, 10, 18, 50]

$$\Gamma = \oint_c \boldsymbol{v}_{ext} \cdot d\boldsymbol{\ell} = \pm\frac{2\pi}{M_{Ps}}. \tag{B.3}$$

This result is true for any counterclockwise contour of enclosing the isolated first-order zero in $f_{Ps}(\kappa_z, \kappa_x)$ provided there are no other zeros enclosed in the contour. The plus sign corresponds to a counterclockwise rotation of $\boldsymbol{v}_{ext}$, whereas the minus sign corresponds to a clockwise rotation.

The non-zero circulation and the rotation of $\boldsymbol{v}_{ext}$ about the first-order zero in f_{Ps} show that there is a vortex in $\boldsymbol{v}_{ext}$. Using the form of f_{Ps} in the vicinity of the first-order zero, equation (B.1), one obtains for the expectation value of the angular momentum operator,

$$\begin{aligned}\langle \boldsymbol{L}\rangle_A = \hat{\boldsymbol{y}}\,\langle L_y\rangle_A &= \hat{\boldsymbol{y}}\,\frac{\int_A f_{Ps}^*(\kappa_z, \kappa_x) L_y f_{Ps}(\kappa_z, \kappa_x) d\kappa_z' d\kappa_x'}{\int_A |f_{Ps}(\kappa_z, \kappa_x)|^2 d\kappa_z' d\kappa_x'} \\ &\approx \hat{\boldsymbol{y}}\,\frac{2\,\mathrm{Im}[b]}{1 + |b|^2},\end{aligned} \tag{B.4}$$

where A is the area of a small square or of a small circle, both with center at the zero in f_{Ps} [3, 9]. The expectation value $\langle L_y\rangle_A$ is nonzero since $\mathrm{Im}[b] \neq 0$. It is positive for $\mathrm{Im}[b] > 0$, which is for counterclockwise rotation of $\boldsymbol{v}_{ext}$, and negative for $\mathrm{Im}[b] < 0$.

ORCID iDs

S J Ward https://orcid.org/0000-0002-8496-360X

References

[1] Macek J H, Sternberg J B, Ovchinnikov S Y and Briggs J S 2010 Theory of deep minima in $(e, 2e)$ measurements of triply differential cross sections *Phys. Rev. Lett.* **104** 033201
[2] Murray A J and Read F H 1993 Evolution from the coplanar to the perpendicular plane geometry of helium $(e, 2e)$ differential cross sections symmetric in scattering angle and energy *Phys. Rev.* A **47** 3724–32
[3] Ward S J and Macek J H 2014 Effect of a vortex in the triply differential cross section for electron impact K-shell ionization of carbon *Phys. Rev.* A **90** 062709
[4] Navarrete F, Della Picca R, Fiol J and Barrachina R O 2013 Vortices in ionization collisions by positron impact *J. Phys. B: At. Mol. Opt. Phys.* **46** 115203
[5] Navarrete F and Barrachina R O 2015 Vortices in the three-body electron-positron-proton continuum system induced by the positron-impact ionization of hydrogen *J. Phys. B: At. Mol. Opt. Phys.* **48** 055201
[6] Navarrete F and Barrachina R O 2016 Vortices in ionization collisions *Nucl. Instrum. Methods Phys. Res.* B **369** 72–6

[7] Navarrete F and Barrachina R O 2017 Vortices rings in the ionization of atoms by positron impact *J. Phys.: Conf. Ser.* **875** 012022

[8] Macek J H, Sternberg J B, Ovchinnikov S Y, Lee T G and Schultz D R 2009 Origin, evolution, and imaging of vortices in atomic processes *Phys. Rev. Lett.* **102** 143201

[9] Macek J H 2013 Peripheral collisions of fast electrons with highly charged ions *AIP Conf. Proc.* **1525** 111–3

[10] Bialynicki-Birula I, Bialynicka-Birula Z and Śliwa C 2000 Motion of vortex lines in quantum mechanics *Phys. Rev.* A **61** 032110

[11] Ovchinnikov S Y, Macek J H and Schultz D R 2014 Hydrodynamical interpretation of angular momentum and energy transfer in atomic processes *Phys. Rev.* A **90** 062713

[12] Ngoko Djiokap J M, Hu S X, Madsen L B, Manakov N L, Meremianin A V and Starace Anthony F 2015 Electron vortices in photoionization by circularly polarized attosecond pulses *Phys. Rev. Lett.* **115** 113004

[13] Ngoko Djiokap J M, Meremianin A V, Manakov N L, Hu S X, Madsen L B and Starace Anthony F 2015 Multistart spiral electron vortices in ionization by circularly polarized UV pulses *Phys. Rev.* A **94** 013408

[14] Larionov N, Ovchinnkov S Y, Smirnovsky A A and Schmidt A A 2018 Perturbation theory in the analysis of quantum vortices formed by impact of ultrashort electromagnetic pulse on atom *Tech. Phys.* **63** 1569–75
Larionov N, Ovchinnkov S Y, Smirnovsky A A and Schmidt A A 2018 Original Russian text published in *Zh. Tekh. Fiz.* **88** 1621–7

[15] McCullough E A Jr and Wyatt R E 1971 Dynamics of the collinear H + H_2 reaction. I. Probability density and flux *J. Chem. Phys.* **54** 3578–91

[16] Hirschfelder J O, Christoph A C and Palke W E 1974 Quantum mechanical steamlines. I. Square potential barrier *J. Chem. Phys.* **61** 5435–55

[17] Kuppermann A, Adams J T and Truhlar D G 1973 Streamlines of probability current density and tunneling fractions for the collinear H + H_2 → H_2 + H reaction *8th Int. Conf. Physics of Electronic and Atomic Collisions (VIII ICPEAC)* vol I (*Abstracts of Papers) ed*) ed B C Čobić and M V Kurepa (Institute of Physics: Belgrade, Yugoslavia) pp 149–50

[18] Dirac P A M 1931 Quantised singularities in the electromagnetic field *Proc. R. Soc.* A **133** 60–72

[19] Hirschfelder J O, Goebel C J and Bruch L W 1974 Quantized vortices around wavefunction nodes. II *J. Chem. Phys.* **61** 5456–9

[20] Madelung E 1927 Quantentheorie in hydrodynamischer form (quantum theory in hydrodynamics form) *Z. Phys.* **40** 322–6

[21] Ghosh S K and Deb B M 1982 Densities, density-functionals and electron fluids *Phys. Rep.* **92** 1–44

[22] Wallstorm T C 1994 Inequivalence between Schrödinger equation and the Madeling hydrodynamic equations *Phys. Rev.* A **49** 1613–7

[23] Hushwater V 2010 Comment on 'Inequivalence between the Schrodinger Equation and the Madelung Hydrodynamic Equations' (arXiv:1005.2420v4 [quant-ph])

[24] Kemble E C 1937 *The fundamental Principles of Quantum Mechanics with Elementary Applications* (New York: McGraw Hill)

[25] Dollard J D 1971 Quantum-mechanical scattering theory for short-range and coulomb interactions *Rocky Mt. J. Math.* **1** 5–88

[26] Macek J H 2012 Vortices in atomic processes *Dynamical Processes in Atomic and Molecular Physics* ed G Ogurtsov and D Dowek (Sharjah: Bentham Science) ch 1, pp 3–28

[27] Briggs J S and Feagin J M 2013 Momentum and spatial imaging of multi-fragments dissociation reactions *J. Phys. B: At. Mol. Opt. Phys.* **46** 025202

[28] Briggs J S and Feagin J M 2014 Scattering theory, multiparticle detection, and time *Phys. Rev* A **90** 052712

[29] Armour E A G and Humberston J W 1991 Methods and programs in collisions of positrons with atoms and molecules *Phys. Rep.* **204** 165–251

[30] Humberston J W, Van Reeth P, Watts M S T and Meyerhof W E 1997 Positron-hydrogen scattering in the vicinity of the positronium formation threshold *J. Phys. B: At. Mol. Opt. Phys.* **30** 2477–93

[31] Van Reeth P and Humberston J W 1998 The energy dependence of the annhilation rate in positron-atom scattering *J. Phys. B: At. Mol. Opt. Phys.* **31** L231–8

[32] Shipman M, Armitage S, Beale J, Brawley S J, Fayer S E, Garner A J, Leslie D E, Van Reeth P and Laricchia G 2015 Absolute differential positronium-formation cross section *Phys. Rev. Lett.* **115** 03340

[33] Drachman R J, Omidvar K and McGuire J H 1976 Differential cross section for positronium formation in positron-atomic-hydrogen collisions *Phys. Rev.* A **14** 100–3

[34] Chan Y F and Fraser P A 1973 *S*-wave positron scattering by hydrogen atoms *J. Phys. B: At. Mol. Phys.* **6** 2504–15

[35] Chan Y F and McEachran R P 1976 Inelastic *P*-wave positron-hydrogen scattering *J. Phys. B: At. Mol. Phys.* **9** 2869–75

[36] Mandal P, Guha S and Sil N C 1979 Positronium formation in positron scattering from hydrogen and helium atoms: the distorted-wave approximation *J. Phys. B: At. Mol. Phys.* **12** 2913–24

[37] Charlton M and Humberston J W 2001 *Positron Physics* (Cambridge: Cambridge University Press)

[38] Woods D, Ward S J and Van Reeth P 2015 Detailed investigation of low-energy positronium-hydrogen scattering *Phys. Rev.* A **92** 022713

[39] Schwartz C 1961 Electron scattering from hydrogen *Phys. Rev.* **124** 1468–71

[40] Schwartz C 1961 Variational calculations of scattering *Ann. Phys.* **16** 36–50

[41] Bransden B H 1970 *Atomic Collision Theory, Lecture Notes and Supplements in Physics* (New York: Benjamin)

[42] Van Reeth P, Woods D, Ward S J and Humberston J W 2016 Comparison of positronium, positron and electron collisions with hydrogen at low velocities *J. Phys. B: At. Mol. Opt. Phys.* **49** 114001
Van Reeth P, Woods D, Ward S J and Humberston J W 2016 Corrigendum *J. Phys. B: At. Mol. Opt. Phys.* **49** 169501

[43] Schwartz C 1961 Lamb shift in the helium atom *Phys. Rev.* **123** 1700–5

[44] Colgan J, Al-Hagan O, Madison D H, Murray A J and Pindzola M S 2009 Deep interference minima in non-coplanar triple differential cross sections for the electron-impact ionization of small atoms and molecules *J. Phys. B: At. Mol. Opt. Phys.* **42** 171001

[45] Feagin J M 2011 Vortex kinematics of a continuum electron pair *J. Phys. B: At. Mol. Opt. Phys.* **44** 011001

[46] Ward S J and Van Reeth P 2016 Deep minimum in the differential cross section for Ps formation in positron-hydrogen *Bull. Am. Phys. Soc.* **61** Q1 26 193
Ward S J, Van Reeth P and Alrowaily A W 2017 Vortices for Ps formation in positron-hydrogen collisions *Bull. Am. Phys. Soc.* **62** K1 148 137 (http://meetings.aps.org/link/BAPS.2017.DAMOP.K1.148) (http://absimage.aps.org/image/DAMOP17/MWS_DAMOP17-2017-000128.pdf)
Van Reeth P, Alrowaily A W, Ward S J and Hiley B J 2017 *Vortices in Low-Energy Positron-Hydrogen Collisions* (http://emqm17.org/poster-session/Peter-van-Reeth-1/)

Ward S J, Alrowaily A W and Van Reeth P 2018 Vortices for Ps formation in positron-hydrogen collisions in the Ore gap *Bull. Am. Phys. Soc.* **63** T01 31 189 (http://meetings.aps.org/Meeting/DAMOP18/Session/T01.31) (http://absimage.aps.org/image/DAMOP18/MWS_DAMOP18-2018-000047.pdf)

Ward S J, Alrowaily A W and Van Reeth P 2018 Ring vortices for positronium formation in positron-hydrogen collisions *18th International Conference on Positron Annihilation, Book of Abstracts, book-revised.pdf* 72 (https://www.bgsu.edu/icpa18.html)

Ward S J, Alrowaily A W and Van Reeth P 2018 Ring vortices for positronium formation in positron-hydrogen collisions in the Ore gap *Abstract for the 71st Annual Gaseous Electronics Conference (GEC) Meeting of the American Physical Society* (http://meetings.aps.org/Meeting/GEC18/Session/GT1.3) (http://absimage.aps.org/image/GEC18/MWS_GEC18-2018-000100.pdf)

Ward S J, Alrowaily A W and Van Reeth P 2019 Multichannel effective range theory analysis of zeros in the positronium formation scattering amplitude for positron-hydrogen collisions *Bull. Am. Phys. Soc.* **64** E01 32 50–1 (http://meetings.aps.org/Meeting/DAMOP19/Session/E01.32) (http://absimage.aps.org/image/DAMOP19/MWS_DAMOP19-2019-000075.pdf)

Alrowaily A W, Ward S J and Van Reeth P 2019 Deep minima and vortices for positronium formation in positron-hydrogen collisions *XX International Workshop on Low-Energy Positron and Positronium Physics, POSMOL 2019 Book of Abstracts, LEPPP* 11 52 (http://posmol2019.ipb.ac.rs/_files/Book_ POSMOL2019_ Online.pdf)

[47] Wolfram Research Inc., Mathematica, Champaign, IL

[48] Hirschfelder J O and Tang K T 1976 Quantum mechanical streamlines. III. Idealized reactive atom-diatomic molecule collisions *J. Chem. Phys.* **64** 760–85

[49] Hirschfelder J O 1977 The angular momentum, creation, and significance of quantized vortices *J. Chem. Phys.* **67** 5477–83

[50] Kan K K and Griffin J J 1977 Single-particle Schrödinger fluid *Phys. Rev.* C **15** 1126–51

[51] Ross M H and Shaw G L 1961 Multichannel effective range theory *Ann. Phys.* **13** 147–86